

Synthesis and characterization of nanowires formed by self-assembled iron particles

J Knipping¹, H Wiggers¹, B F Kock¹, T Hülser², B Rellinghaus^{1,3}
and P Roth^{1,4}

¹ Institute for Combustion and Gasdynamics, University of Duisburg-Essen, 47048 Duisburg, Germany

² Experimental Physics, University of Duisburg-Essen, 47048 Duisburg, Germany

E-mail: knipping@uni-duisburg.de and roth@ivg.uni-duisburg.de

Received 19 August 2004, in final form 24 September 2004

Published 22 October 2004

Online at stacks.iop.org/Nano/15/1665

doi:10.1088/0957-4484/15/11/051

Abstract

The formation of iron particles without and with carbon coating was studied in a hot wall flow reactor. The precursors ironpentacarbonyl (IPC, $\text{Fe}(\text{CO})_5$) and ethylene (C_2H_4) both diluted in N_2 were used in a concentric tubular flow arrangement and were heated to temperatures between 570 and 1170 K at pressures between 50 and 500 mbar. In experiments without C_2H_4 , either individual iron particles in the size range of $8 \text{ nm} \leq d_p \leq 15 \text{ nm}$ or long iron chains composed of several hundreds of individual iron particles were found depending on the reaction conditions. In experiments with C_2H_4 addition, these particles or particle chains were covered by a thin carbon/carbide layer. The size of the primary particles was measured *in situ* by time-resolved laser-induced incandescence (TR-LII) and *ex situ* by rapid thermophoretic particle probing and TEM imaging.

1. Introduction

Iron is one of the most widely used materials in the technological world. In recent years, nanostructured materials and nanoparticles have opened the possibility of new far-reaching usage of old materials. This is mostly a result of size effects which can drastically modify the bulk material properties. Also, iron and iron oxides are in this context of interest because of the size-dependent magnetic, electronic, and catalytic properties. Various gas phase (aerosol) synthesis routes [1–6], are known, by which precursors can be transformed via chemical and physical rate processes into nanoparticles, e.g. flames, laser reactors, plasma reactors, and hot wall reactors.

The synthesis of iron particles via the gas phase route is strongly controlled by both the decomposition of the precursor and the single-iron-cluster formation and growth [7–9]. An aerosol model for the formation of iron particles

was introduced by Bilodeau and Proulx [10] and by Giesen *et al* [11]. As iron particles are very reactive, showing e.g. spontaneous oxidation in air, it is useful to cover the particle surface by a thin oxidic layer or to encapsulate the particles e.g. by a carbon/carbide shell.

In the present paper, the synthesis of iron particles by thermal decomposition of ironpentacarbonyl ($\text{Fe}(\text{CO})_5$) in a hot wall flow reactor is reported. The reaction has some interesting features: the decomposition starts at very low temperatures and a complete conversion of the precursor without the formation of by-products can be achieved. The lifetime of $\text{Fe}(\text{CO})_5$ at 570 K has been measured to be 5.3 ms [12]. The relative ease of scaling up hot wall reactors qualifies this production route for industrial purposes. Even with the present set-up, production rates in the range of 1–2 g h^{-1} have been realized. The size of the synthesized particles was determined *in situ* by time-resolved laser-induced incandescence (TR-LII). Size distribution and particle morphology was also examined by rapid thermophoretic particle sampling and visualization by transmission electron

³ Current address: IFW Dresden eV, 01069 Dresden, Germany.

⁴ Author to whom any correspondence should be addressed.

microscopy (TEM). The role of the second precursor C_2H_4 used in an additional series of experiments was unclear when starting these measurements. In the temperature/residence time window of the present study, a significant homogeneous thermal decomposition of C_2H_4 is very unlikely. On the other hand, the surface of the iron particles can catalyse C_2H_4 reactions resulting in carbon layers or C–Fe reactions.

2. Experimental details

2.1. Hot wall flow reactor

The experimental set-up used in the present study is schematically shown in figure 1. It consists of a hot wall flow reactor to produce the particles, a TR-LII measurement system connected at the end of the flow tube for *in situ* particle sizing, a rapid thermophoretic TEM probing system, and a filter for collecting the particles. The flow reactor consists of three concentric tubes, which are positioned inside a tubular furnace. Mixing and heat-up of the precursor flows can be varied by relative shift of the concentric tubes. The $Fe(CO)_5/N_2$ mixture enters the reactor through a nozzle which is situated inside the main reaction tube of 22 mm inner diameter and located 200 mm above the furnace. The C_2H_4/N_2 mixture enters the reaction tube at the top of the reactor above the furnace. At the exit of the reaction tube outside the furnace, the gas/particle flow can be quenched or diluted by a N_2 flow to avoid particle deposition at the wall and to stop sintering. The particles produced during the material synthesis were collected in a ceramic filter element made of sintered silicon carbide. The total flow rate through the reactor was around 10 L min^{-1} (standard conditions) and the pressure was varied between 50 and 500 mbar.

The temperature was measured along the reactor axis by several thermocouples, but only the mean furnace temperature will be given later. Depending on reaction conditions, the temperature profile of the fluid has its maximum between half the length and the end of the furnace and is about 10% below the indicated furnace temperature. The fluid temperature at the nozzle inlet is about 300 K for a furnace temperature of 670 K. All gas flows were controlled by mass flow meters. The precursor $Fe(CO)_5$ was introduced into the reactor by bubbling nitrogen through a flask containing liquid $Fe(CO)_5$. The flow rate of $Fe(CO)_5$ was calculated from the measured weight loss of the flask during operation.

2.2. TR-LII and TEM probing system

At the exit of the reaction tube (see figure 1) both the *in situ* time-resolved laser-induced incandescence (TR-LII) diagnostic and a rapid TEM probing system are adopted to the measurement chamber. The TR-LII experiments allow the determination of the particle size by heating the particles due to a short laser pulse and recording the complete time-dependent particle emission during particle cooling [13]. From the measured cooling curves, particle size information can be obtained, as larger particles need a longer period to cool down than smaller ones. In the present case, the particles are heated by a Nd:YAG laser with a wavelength of 1064 nm and a pulse time of 8 ns, which crosses the particle–gas stream perpendicular. The pulse energy was adjustable between 50

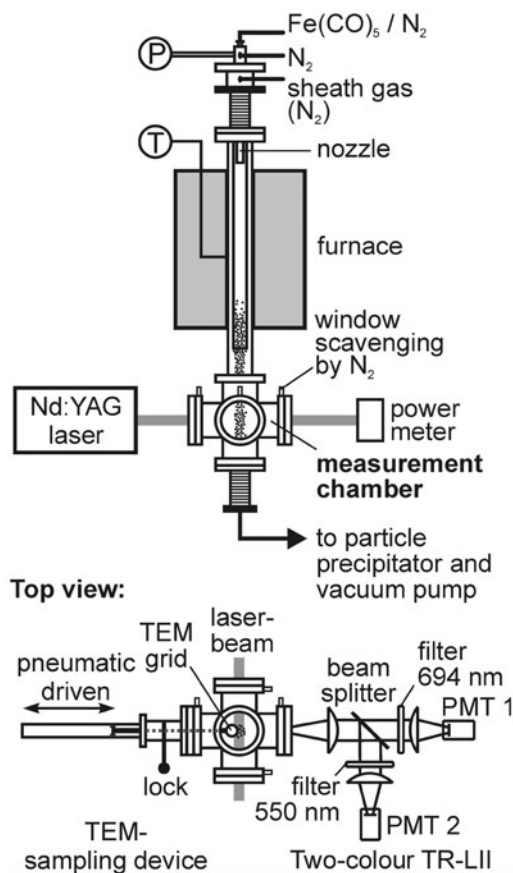


Figure 1. Experimental set-up with hot wall flow reactor, TR-LII measurement technique, and thermophoretic particle sampling.

and 300 mJ/pulse , which corresponds to a fluence of about 0.1 and 1 J cm^{-2} at a screened off laser beam diameter of 6.5 mm . The optical detection system is arranged perpendicular to the laser beam axis and is composed of an optical lens, which collects the thermal emission of the particles and a following beam splitter; see figure 1. Narrow band pass filters with centre-wavelengths of 550 and 694 nm are placed in each beam to limit the radiation to a small spectral range. Finally, two further collecting lenses focus the beams on the photo-cathodes of two high-speed photo-multipliers with integrated amplifiers. The signals were digitized and stored by a digital storage oscilloscope at a sample rate of 5 Gs , corresponding to a time resolution of 0.2 ns . For particle size evaluation the signal at 550 nm is used, while the second signal at 694 nm is utilized to determine the particle heat-up temperature by two-colour pyrometry.

The pneumatic particle sampling system (see figure 1) is comparable to that of Dobbins and Megaridis [14]. It was also adapted to the measurement chamber. A TEM-grid positioned on a holder is mounted on top of the double-acting pneumatic cylinder. It is rapidly moved into the particle flow and removed after a certain precipitation time. The residence time inside the flow is about 150 ms , which ensures minimized heating of the grid and reduced disturbance. In order to avoid uncontrolled pre-deposition of particles during the experiment, the pneumatic cylinder is separated from the reaction tube by a vacuum slide. The sampled particles were visualized by transmission electron microscopy. Resulting images were

used for particle size measurements. These data were fitted to lognormal size distributions, from which mean particle diameters and standard deviations of the size distribution were extracted.

2.3. Further characterization of the particle material

The filter-collected particles were further analysed by x-ray diffraction (XRD) using Cu K α radiation to identify the phase structures. The microstructures of the particle samples were examined both by TEM and by HRTEM (high resolution transmission electron microscopy) and by TEM-adapted analysing methods, like energy dispersive x-ray-analysis (EDX) and electron energy loss spectroscopy (EELS). The BET specific surface area of collected powder was measured by using the adsorption of nitrogen at 77 K. Assuming spherical, monodisperse particles without pores, the mean particle diameter can be calculated from: $d_p = 6000/(\rho S)$, where d_p is the particle diameter in nanometres, S is the specific surface area in $\text{m}^2 \text{g}^{-1}$, and ρ is the bulk density in g cm^{-3} of the particle material. Magnetic properties were analysed by a superconducting quantum interference device (SQUID).

3. Results and discussion

3.1. Pure individual iron particles and self-assembled particles

In the first series of experiments, pure iron particles were synthesized in the hot wall flow reactor. Initial gas mixtures of N_2 with IPC concentrations of $800 \text{ ppm} \leq [\text{Fe}(\text{CO})_5] \leq 12000 \text{ ppm}$ were used. Temperature, pressure, and flow rate were varied in a wide range of conditions as follows: $570 \text{ K} \leq T \leq 1170 \text{ K}$, $50 \text{ mbar} \leq p \leq 500 \text{ mbar}$, $2 \text{ L min}^{-1} \leq V_g \leq 7 \text{ L min}^{-1}$ (at standard state conditions). In all cases, the thermal decomposition of IPC starts in the upper hot zone of the reactor flow with subsequent nucleation and particle formation. At the lower end of the flow reactor, particles were thermophoretically sampled on grids by the earlier described pneumatic system and subsequently visualized by TEM. Three typical examples of TEM pictures illustrating the size and morphology of particles obtained under the various reaction conditions are shown in figure 2. At low IPC concentration, low pressure and high flow rate, individual, nearly spherical particles were obtained; see figure 2(a). At lower temperature and flow rate, the particles are higher aggregated showing loosely structured agglomerates, see figure 2(b). At high IPC concentration and at higher pressure, long particle chains were obtained, see figure 2(c), having a chain length of several micrometres. To make clear that these chains were formed in the gas phase and not on the TEM grid, holey carbon grids have been used.

From the practical point of view, the individual iron particles (figure 2(a)) and the particle chains (figure 2(c)) are of interest and were therefore further analysed. In the case of the individual, nearly spherical particles, the TEM images were analysed by counting the number and diameter of the individual discs. A typical result is shown in the form of a histogram in figure 3. These data were fitted by a lognormal size distribution function (see the curve in

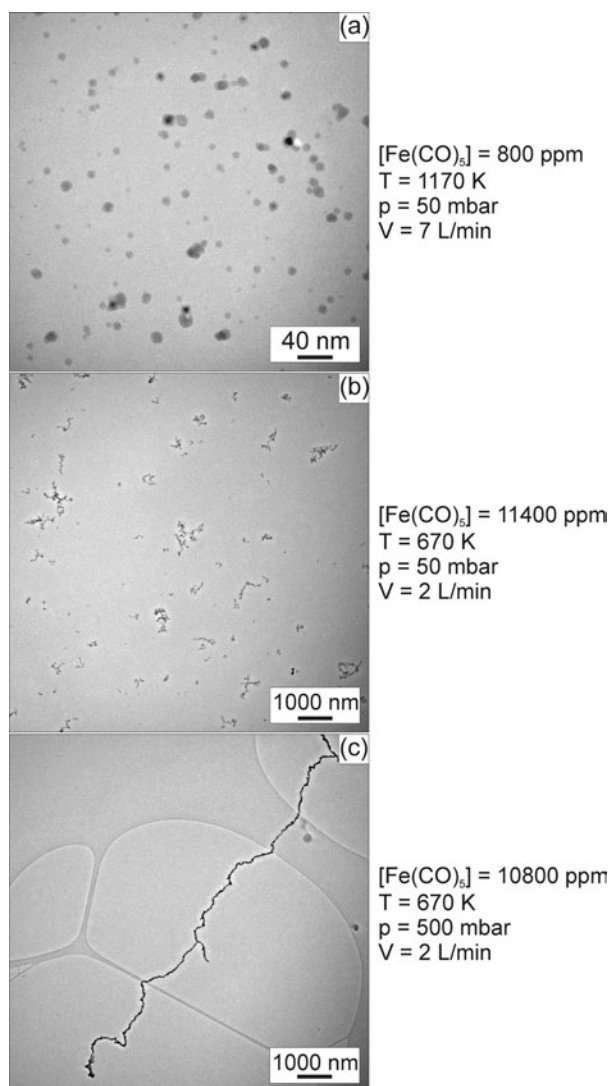


Figure 2. Examples of TEM images of thermophoretically sampled particles by a rapid pneumatic probing system.

figure 3) to determine the count median diameter (CMD) and the geometric standard deviation (σ_g) [15]. In the present example, the values are $\text{CMD} = 9.1 \text{ nm}$ and $\sigma_g = 1.5$. For a group of experiments, the trends in CMD for the lowest pressure experiments as a function of IPC concentration and temperature were determined. Under these conditions, either individual particles or very loose agglomerates were obtained, for which the CMD of the primary particles increases from about $\text{CMD} = 7.5 \text{ nm}$ to about $\text{CMD} = 15 \text{ nm}$ for the higher IPC concentration. The temperature effect is less distinct, which is somewhat surprising.

The most interesting iron particles are those forming long chains by self-assembly in the gas phase. They only appear at the highest pressure and IPC concentration of the present study. According to figure 4(a) the size of the primary particles in such chains is $d_p > 30 \text{ nm}$ and they have a more rectangular, crystalline form; see the inset of figure 4(a). TR-LII measurements were performed and the exciting question is what is in this case the answer obtained from particle emission. A typical, normalized TR-LII signal (only the cooling part) obtained from the iron chains is shown in figure 4(b) (noisy

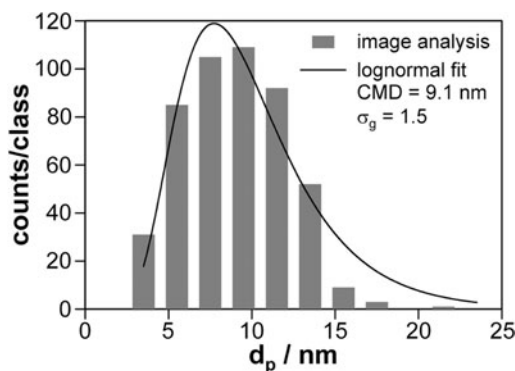


Figure 3. Size distribution of evaluated TEM image (histogram) and lognormal size distribution fit.

grey graph). According to Kock *et al* [13], the curve was fitted by an extended heat transfer model assuming point contact between the particles of the chain. By varying the CMD of the primary particles and the translational energy accommodation coefficient α_T , the black curve in figure 4(b) was obtained as a best fit with values of CMD = 34.6 nm and $\alpha_T = 0.15$. The CMD result is very close to the value determined from the TEM picture (CMD = 36 nm). Similar results were obtained for other flow and reaction conditions with slightly different chain structures.

The remaining question is what is the driving potential that either individual particles or long particle chains are formed in the reactive flow. It is very likely that the magnetic properties play a role. A closer look with the HRTEM at the morphology indicates differences: The small individual particles of $d_p < 15$ nm are more spherical; the primary particles in a chain ($d_p > 20$ nm) have a faceted structure. It is known that magnetic particles show strong size effects. It can be calculated [16] that iron particles with $d_p < 16$ nm are superparamagnetic at $T > 300$ K, e.g. they do not carry a remanent magnetization since the magnetization direction is unstable due to thermal fluctuation. Iron particles in the size range $d_p > 16$ nm are ferromagnetic but still small enough to be single magnetic domains. In other words: they behave like permanent magnets. This has consequences for the particle behaviour in the reactive flow. Beside van der Waals forces, the magnetic forces between the particles seem to dominate the collision behaviour. The particles have a certain mobility in the gas suspension and stick together in the direction of the magnetic dipoles of the primary particles. This leads to the observed self-assembling into long chains with probably further internal sintering. The assumption of magnetic forces dominating the collision behaviour can be assisted by an estimation of the order of magnitude of the magnetic F_m and van der Waals forces F_W using functions given by Cullity [16] and Friedlander [17]. Assuming 30 nm iron particles separated by a distance of 1 nm, the estimated values are $F_m \approx 10^{-7}$ N and $F_W \approx 10^{-10}$ N, respectively.

The particle material, produced under the various operation conditions in the flow reactor, was further characterized by various *ex situ* methods (XRD, EDX, EELS, BET, SQUID). The details can only be described without showing the various graphs. The material is mostly α -Fe with a thin layer of γ -Fe₂O₃ originating from handling in

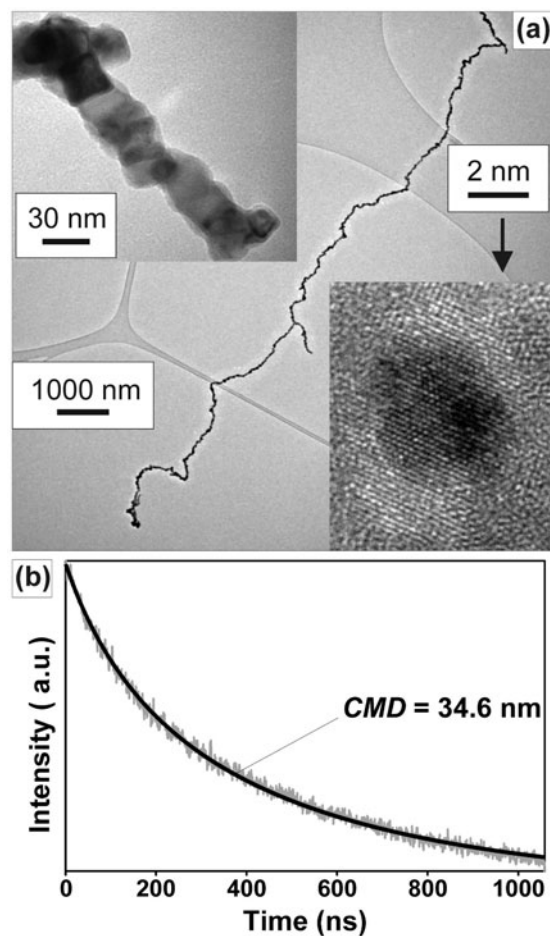


Figure 4. (a) TEM/HRTEM structure of iron particle chains. (b) Normalized TR-LII rough signal (noisy line) and fitted curve (drawn line) based on an extended heat transfer model.

air. This thin, stable oxidation layer seems to prevent the iron particles from self-ignition. The magnetic measurements reveal superparamagnetic behaviour of small particles at $T > 200$ K. The lattice parameters determined from HRTEM images correlate either with iron or with iron oxide. The BET measurements confirm the measurements by TEM and TR-LII.

3.2. Carbon/carbide coated individual iron particles and particle chains

In the second series of experiments, particles were synthesized in the hot wall flow reactor under conditions given earlier except C₂H₄, which was added to the precursor gas flow in relative concentrations of $1/14 \leq [\text{IPC}]/[\text{C}_2\text{H}_4] \leq 1/1$. Although homogenous thermal decomposition of C₂H₄ is very unlikely under the temperature conditions used in the present experiments, the surface of iron particles can catalyse C₂H₄ reaction by which either elementary carbon or Fe/C-products can be formed. To make sure that the C₂H₄ addition does not significantly change the overall morphology of the particles formed in the hot wall flow reactor, experiments were performed under conditions similar to those of figures 2(a) and (c). Particles thermophoretically sampled on grids are shown in the TEM images of figure 5. Although the resolution is not high, a clear core-shell-structure of the individual,

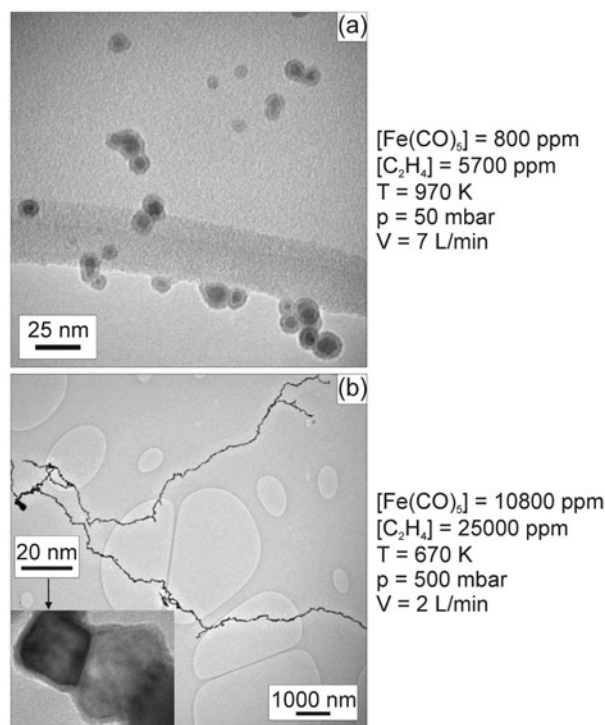


Figure 5. Examples of carbon/carbide coated iron particles. (a) Spherical individual particles. (b) Particle chains.

spherical particles in figure 5(a) is visible. In this example the determined mean particle size is $d_p \approx 12 \text{ nm}$ ($d_{\text{core}} \approx 7 \text{ nm}$, $t_{\text{shell}} \approx 2.5 \text{ nm}$, d_{core} is the diameter of the core and t_{shell} is the thickness of the shell). Reactor experiments under conditions where particle chains must be expected again show chains formed by self-assembly of the individual particles; see figure 5(b). The inset in figure 5(b) clearly shows the particle coating. The overall chain length obtained is similar to the previous experiments without C_2H_4 addition.

A better insight into the detailed particle structure was obtained from HRTEM images and from EELS line scans over individual particles. Such measurements are somewhat difficult to perform due to particle drift and interferences between the electron beam and the magnetic particles, especially with the chainlike particles. Figure 6(a) shows a STEM picture (scanning transmission electron microscopy) of neighbouring spherical particles with diameter $d_p \approx 9 \text{ nm}$. The core-shell structure is clearly visible and is further confirmed by the EELS line scan; see the inset of figure 6(a) and the graph in figure 6(b). The intensity profiles show carbon peaks in the surface region of the particle and an Fe maximum in the particle core. The C signal cannot completely disappear in the particle centre because the electron beam always passes the outer carbon/carbide layer of the spherical structure. The EELS spectrum also shows some oxygen to be present, which originates from exposure to air. Other experiments which we cannot show in detail revealed a strong relation between the C_2H_4 concentration in the precursor gas and the thickness of the particle shell. For reaction conditions $[\text{IPC}]/[\text{C}_2\text{H}_4] = 1/1$, the iron particle shell is very thin and difficult to visualize, whereas for higher relative C_2H_4 concentrations of $[\text{IPC}]/[\text{C}_2\text{H}_4] = 1/7$ or $1/14$ the particle

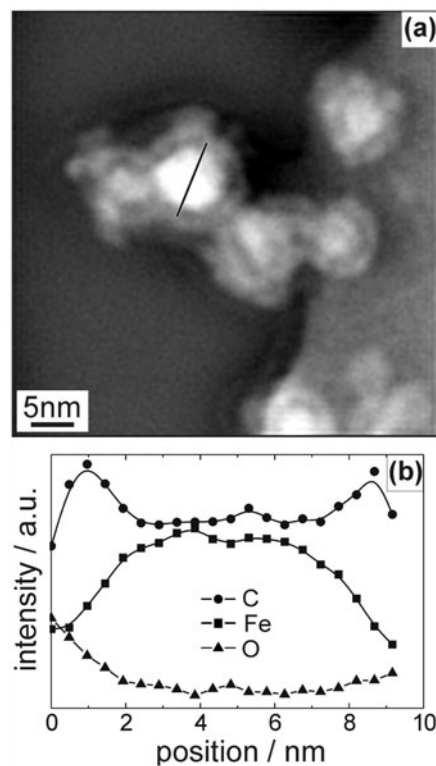


Figure 6. (a) STEM of coated iron particles. (b) EELS line scan over an individual particle.

shell was found to be up to 3 nm thick. The core-shell structure of the particle chains was also further analysed by HRTEM and by EELS. The results are more or less the same as illustrated for the spherical primary particles.

The nature of the layer by which the iron nanoparticles are covered is not completely clear up to now. XRD spectra of particle powder, which are not sensitive to amorphous carbon, revealed strong peaks of $\alpha\text{-Fe}$ and weak indications of Fe_3C (iron carbide). These data are assisted by Mössbauer spectroscopy, which reveals the existence of iron carbide, $\alpha\text{-Fe}$, and a certain amount of magnetite. We speculate from all the various observations that the particle formation process proceeds in the following steps: from the two precursors, IPC starts to decompose in the upper part of the reactor at considerably low temperature. The process of iron nucleation and iron particle formation proceeds very rapidly with collision frequency. During this process, the interference with catalytic reactions of C_2H_4 at the rapidly formed iron surface must be low. C_2H_4 catalysis seems to become significant later in the reacting flow, as soon as the iron particles and their catalysing surface are further developed and the gas phase has been heated up to a certain catalysis-starting temperature. The carbon atoms present at the outer surface diffuse into the Fe particles, forming Fe carbides.

3.3. Further preliminary test on iron particle chains

A certain amount of powder composed of self-assembled iron particles (without carbon coating) was produced under reaction conditions described earlier. The powder was dispersed in ethanol, later deposited on a silicon substrate, and visualized

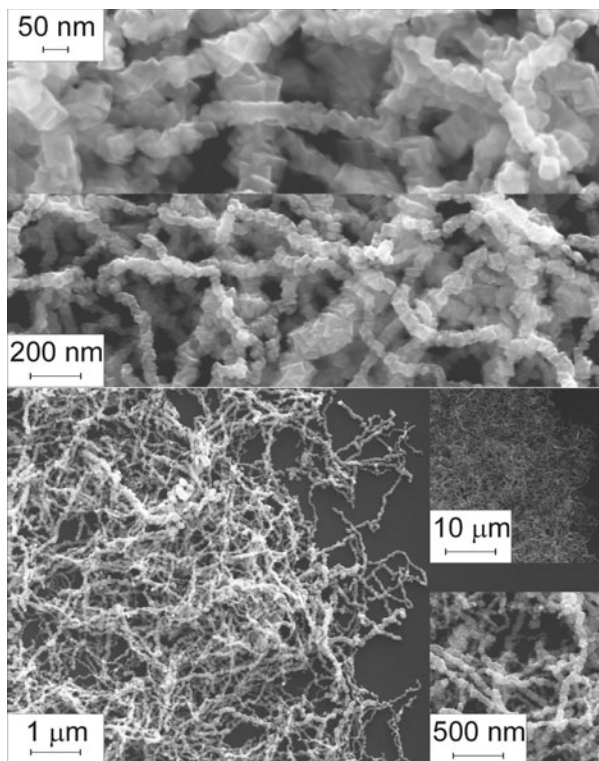


Figure 7. SEM images of iron chains deposited on silicon substrate from dispersion of powder product in ethanol.

by SEM analysis. The result is shown in figure 7 in various magnifications. A dense network of chain structures can be seen with individual primary particles still being observable. They are surprisingly equal in size. The handling of the powder seems not to affect or destroy the formed chain structures. The random organized network of particle chains and their highly accessible surface implies applications such as filtering or catalysis.

In further experiments, individual iron particle chains were deposited by use of the pneumatic probing device on interdigital capacitor (IDC) structures; see figure 8 (a part of an IDC is shown in the upper left corner of figure 8). The SEM images clearly reveal the faceted, nearly cubic structure of the primary particles. The aim is to characterize a single iron chain as well as an array of chains to discover possible applications in the range of conductive nanowires. First current–voltage spectra on multiple iron chains indicate an ohmic behaviour. Measurements on the powder product pressed in pellets show a specific DC resistance of $P = 8 \Omega \text{ m}$. The electrical characterization by experiments with a conducting AFM (atomic force microscope) are in progress. With this instrument the conductivity of a single nanowire can be determined.

4. Conclusion

Iron nanoparticles in the size range $8 \text{ nm} \leq d_p \leq 35 \text{ nm}$ were synthesized in a hot wall flow reactor by thermal decomposition of ironpentacarbonyl (IPC, $\text{Fe}(\text{CO})_5$). Depending on the reaction conditions, either individual

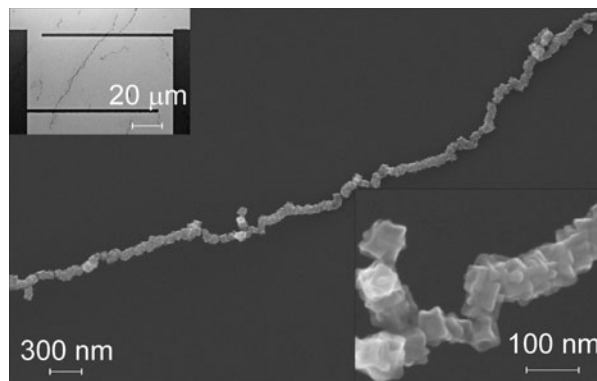


Figure 8. SEM images of iron chains deposited thermophoretically on IDC structure.

particles with $8 \text{ nm} \leq d_p \leq 15 \text{ nm}$ or long chains formed by self-assembly and composed of up to 400 primary particles with $d_p \approx 30 \text{ nm}$ were found. The formation of such long particle chains must be a result of self-organization driven by magnetic dipole forces. Other reactor experiments with mixtures of IPC and C_2H_4 diluted in N_2 revealed iron particles or iron chains covered by a carbon/carbide shell. The thickness of the carbon or the Fe carbide layer depends on the mixture ratio of IPC and C_2H_4 . The detailed structure of the shell layer could up to now not be classified with certainty. Such coated iron particles are expected to find possible application in magnetic fluids or in magneto-thermography.

Acknowledgments

The financial support of the ‘Deutsche Forschungsgemeinschaft’ is gratefully acknowledged. The authors would like to thank Dr Mehmet Acet and Eyup Duman for performing the magnetic measurements.

References

- [1] Kalyanaraman R, Yoo S, Krupashankara M S, Sudarshan T S and Dowding R J 1998 *Nanostruct. Mater.* **10** 1379
- [2] Janzen C and Roth P 2001 *Combust. Flame* **125** 1150
- [3] Orthner H R and Roth P 2002 *Mater. Chem. Phys.* **78** 453
- [4] Pratsinis S E and Vemury S 1996 *Powder Technol.* **88** 267
- [5] Brezinsky K 1996 *Proc. Combust. Inst.* **26** 1805
- [6] Wooldridge M S 1998 *Prog. Energy Combust. Sci.* **24** 63
- [7] Bauer S H and Frurip D J 1977 *J. Phys. Chem.* **81** 1015
- [8] Jensen D E 1980 *J. Chem. Soc. Faraday Trans. 2* **76** 1494
- [9] Giesen A, Herzler J and Roth P 2003 *J. Phys. Chem. A* **107** 5202
- [10] Bilodeau J-F and Proulx P 1996 *Aerosol Sci. Technol.* **24** 175
- [11] Giesen A, Kowalik A and Roth P 2004 *Phase Transit.* **77** 115
- [12] Didenkulova I I, Pereplechikov M L and Aleksandrov Y A 1990 *Russ. J. Phys. Chem.* **64** 1836 (Engl. Transl.)
- [13] Kock B F, Kayan C, Knipping J, Orthner H R and Roth P 2004 *Proc. Combust. Inst.* **30** at press
- [14] Dobbins R A and Megaridis C M 1987 *Langmuir* **3** 254
- [15] Hinds W C 1982 *Aerosol Technology* (New York: Wiley)
- [16] Cullity B D 1972 *Introduction to Magnetic Materials* (Menlo Park, CA: Addison-Wesley)
- [17] Friedlander S K 2000 *Smoke, Dust, and Haze* (New York: Oxford University Press)